Available online at www.sciencedirect.com
SCIENCE DIRECT®
International Journal of Heat and Mass Transfer 47 (2004) 5501–5509
International Journal of HEAT and MASS TRANSFER
www.elsevier.com/locate/ijhmt

Numerical simulation of the Czochralski growth process of oxide crystals with a relatively thin optical thickness

Akira Hayashi, Masaki Kobayashi, Chengjun Jing, Takao Tsukada *, Mitsunori Hozawa

Institute of Multidisciplinary Research for Advanced Materials, Tohoku University, 2-1-1 Katahira, Aoba-ku, Sendai 980-8577, Japan

Received 3 April 2003; received in revised form 2 June 2004
Available online 16 September 2004

Abstract

For the single crystal growth of an oxide, the global analysis of heat transfer in the inductively heated Czochralski (CZ) furnace was carried out to investigate the effect of optical properties of crystal on the CZ crystal growth process. Here, the finite volume method (FVM) was used as the radiative transfer model to solve the radiative transfer equation, and consequently the crystal with a relatively thin optical thickness (~0.01) could be accounted for. As a result, it was found that the melt/crystal interface becomes more convex toward the melt for a small crystal rotational Reynolds number as the optical thickness of the crystal, κ_s, decreases, although its dependence is slight for $\kappa_s < 0.1$. In addition, the critical Reynolds number, at which the interface inversion occurs, decreases with the optical thickness of the crystal.

1. Introduction

Oxide single crystals such as yttrium aluminum garnet, gadolinium gallium garnet and lithium niobate are utilized as solid-state laser hosts and materials for acousto-optic-electronic devices, and are commonly grown by the Czochralski (CZ) method. For the production of a perfect oxide single crystal by the CZ method, it is important to acquire accurate information about the heat transfer mechanism and then to control the heat transfer in the CZ furnace, because the quality of the crystal is closely related to its thermal history and the transport phenomena in the furnace.

Oxide single crystals are not opaque to infrared radiation, so the radiative heat absorption and emission in the crystal strongly influence the heat transfer behavior and the shape of the melt/crystal interface during the CZ crystal growth. For example, it is experimentally known that the radiative heat transfer through the crystal renders the interface deeply convex toward the melt [1,2], and that the change in the absorption coefficient of the crystal affects the growth characteristics [3,4]. Recently, such influences of the radiative heat transfer in the oxide crystal on the crystal growth behavior have also been demonstrated numerically with the global analysis of heat transfer [5–7].

We have also investigated the effect of radiative heat transfer using the global model in which we can predict the electromagnetic, flow, temperature and thermal stress fields in the CZ furnace and the melt/crystal and melt/gas interface shapes as well as the radiative heat transfer in the crystal and/or melt [8,9]. Here, since the P_1 or Milne–Eddington, approximation which is not very well adapted for optically thin materials was used

* Corresponding author. Tel./fax: +81 22 217 5651.
E-mail address: tsukada@tagen.tohoku.ac.jp (T. Tsukada).

0017-9310/$ - see front matter © 2004 Elsevier Ltd. All rights reserved.
doi:10.1016/j.ijheatmasstransfer.2004.06.036

Nomenclature

a'	absorption coefficient (m^{-1})
C'_p	heat capacity ($J\,kg^{-1}\,K^{-1}$)
D	product of the unit normal vector at the surface and intensity direction
$\boldsymbol{e}$	unit vector
F_{jk}	view factor
g'	gravitational acceleration ($m\,s^{-2}$)
Gr	Grashof number ($=\beta' T'_m g' r'^3_c/\nu'^2_l$)
$\Delta H'_f$	latent heat of solidification ($J\,kg^{-1}$)
I'	radiant intensity ($W\,m^{-2}$)
I	$=I'/\sigma' T'^4_m$
J'	irradiance ($W\,m^{-2}$)
J	$=J'/\sigma' T'^4_m$
K_j	ratio of thermal conductivity ($=k'_j/k'_l$)
k'	thermal conductivity ($W\,m^{-1}\,K^{-1}$)
N_R	radiation–conduction interaction parameter ($=\sigma' T'^3_m r'_c/k'_l$)
n	refractive index
$\boldsymbol{n}$	normal unit vector
Pe	Peclet number ($=\rho'_{0s} C'_{ps} V'_s r'_c/k'_l$)
Pr	Prandtl number ($=\mu'_l C'_{pl}/k'_l$)
Q'_0	standard volumetric heat generation rate ($W\,m^{-3}$)
Q_0	$=Q'_0 r'^2_c/(k'_l\cdot T'_m)$
q'_j	net heat flux due to the incident radiation on jth boundary surface ($W\,m^{-2}$)
$q'_{i,j}$	incident radiative flux on jth boundary surface ($W\,m^{-2}$)
q_j	$=q'_j/\sigma' T'^4_m$
$q_{i,j}$	$=q'_{i,j}/\sigma' T'^4_m$
r'	radial position in cylindrical coordinates (m)
r	$=r'/r'_c$
r'_c	crucible radius (m)
r_s	crystal radius
Re	Reynolds number ($=r'^2_c\Omega'/\nu'_l$)
Re_c	critical Reynolds number
St	Stefan number ($=\Delta H'_f/C'_{ps} T'_m$)
T'	temperature (K)
T	$=T'/T'_m$
T'_m	melting temperature (K)
V'_s	crystal pulling rate ($m\,s^{-1}$)
$\boldsymbol{v}'$	velocity vector ($m\,s^{-1}$)
$\boldsymbol{v}$	$=\boldsymbol{v}' r'_c/\nu'_l$
z'	axial position in cylindrical coordinates (m)
z	$=z'/r'_c$
Δz	axial displacement of the interface

Greek symbols

α	heat generation coefficient
β'	thermal expansion coefficient (K^{-1})
ε	emissivity
ϕ	azimuthal angle (rad)
η	direction cosine along the ϕ-axis
κ	optical thickness ($=a' r'_c$)
μ	direction cosine along the r-axis
μ'	viscosity (Pa s)
ν'	kinematic viscosity ($m^2\,s^{-1}$)
ρ'_0	density ($kg\,m^{-3}$)
ρ	reflectivity
σ'	Stefan–Boltzmann constant ($W\,m^{-2}\,K^4$)
τ	transmissivity
ψ	stream function
ξ	direction cosine along the z-axis
Ω'	crystal rotation rate (s^{-1})
ω	solid angle

Superscripts

H	height
in	inside of boundary surface
m	discrete direction of solid angle
OD	outer diameter
out	outside of boundary surface
T	thickness
$'$	dimensional value

Subscripts

b	blackbody
c	crucible
h	after heater
j	material or surface j
jg	pointing from material j to gas phase
k	material or surface k
l	melt
ls	pointing from melt to crystal
max	maximum value
min	minimum value
s	crystal
sg	pointing from crystal to gas phase
z	z-direction

to solve the radiative transfer equation, the melt and/or crystal with a relatively thick optical thickness were targeted. However, oxide crystals have a wide range of absorption coefficient values, and depending on their values the contributions of radiation to heat transfer and consequently the melt/crystal interface shape vary, such as in Cockayne et al.'s experimental work [1].

The aim of the present work is to improve the global model used in previous works [8,9] by introducing the finite volume method (FVM) to solve the radiative trans-

fer equation, so that the radiative heat transfer in the crystals with a wide range of optical thickness values can be accounted for. Then, using this new laboratory-made global analysis code, the effect of optical thickness of the crystal which is relatively thin on the CZ crystal growth process, e.g., the melt/crystal interface shape, is investigated numerically.

2. Mathematical model

Fig. 1 shows an inductively heated CZ furnace for an oxide single crystal growth, which was taken as an object to develop a global heat transfer model in the present work. Here, a pulling rod usually connected with the crystal through the seed was ignored, and also the shape of the crystal top surface was simplified, i.e., a flat shape without a shoulder. The ac electric current in the coil induces the eddy current in the metal crucible wall, and consequently, the raw material of the crystal inside the crucible is melted by the Joule heating from the eddy current. Therefore, in the global analysis of heat transfer in the inductively heated CZ furnace, the electromagnetic field in the system should be computed first in order to obtain the distributions of the eddy current, i.e., heat power in the crucible and the after heater; then flow and temperature fields in the furnace as well as the shapes of the melt/crystal and melt/gas interfaces are calculated.

In our previous works, we developed a mathematical model with which we can predict the electromagnetic, flow and temperature fields in the furnace and the interface shapes [10], and subsequently extended the model by incorporating the P_1 method to account for the internal radiation within the crystal and/or the melt [8]. However, since the P_1 approximation is not very well adapted for optically thin materials, the optical thickness of the crystal and/or melt was limited to values greater than 1. In the present work, the P_1 method was replaced with the FVM to solve the radiative transfer equation, so that even the crystal with a relatively thin optical thickness can be accounted for. For brevity, mathematical details of the global heat transfer model of the CZ furnace are not included here, but are available in our previous work [8,10]. However, the governing equations for the radiative heat transfer which are based on the FVM are described below.

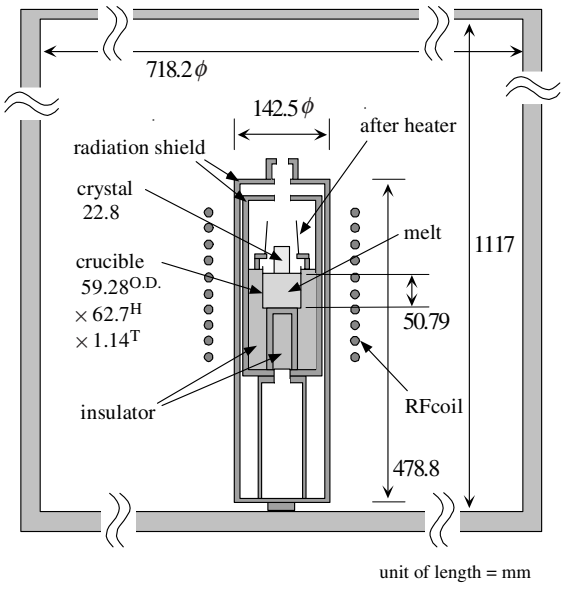

Fig. 1. Schematic diagram of the inductively heated CZ furnace.

Under the assumptions that the system is axisymmetric and in the quasi-steady state, the dimensionless energy equations are given as follows,

$$\text{Melt}: \quad Pr\boldsymbol{v}_l \cdot \nabla T_l = \nabla^2 T_l, \tag{1}$$

$$\text{Crystal}: \quad Pe\boldsymbol{e}_z \cdot \nabla T_s = K_s \nabla^2 T_s + \kappa_s N_R (J_s - 4n_s^2 T_s^4), \tag{2}$$

$$\text{Crucible and after heater}: \quad K_j \nabla^2 T_j + \alpha Q_0 = 0 \quad (j = c, h), \tag{3}$$

$$\text{Elsewhere}: \quad K_j \nabla^2 T_j = 0, \tag{4}$$

where T is temperature and $\boldsymbol{v}$ is the velocity vector governed by the momentum equation. Pr, Pe and K_j are the Prandtl number, Peclet number and thermal conductivity ratios to that of the melt, defined by $\mu_l' C_{pl}'/k_l'$, $\rho_{0s}' C_{ps}' V_s' r_c'/k_l'$ and k_j'/k_l', respectively. Q_0 is the dimensionless heat generation rate by the Joule heat in the crucible and after heater for a reference value of the electric current in the RF coil, and is obtained from the analysis of the electromagnetic field in the furnace. α in Eq. (3) is determined to be a part of the solution so that the temperature at the tri-junction may be the melting point, on the basis of the fact that the local heat generation rate is proportional to the square of the current density in the coil. The subscripts "l, s, c, and h" in the above equations indicate the melt, crystal, crucible and after heater, respectively.

In Eq. (2), the second term on the right-hand side represents the contribution of the radiative heat transfer, in which κ_s and N_R are the optical thickness of the crystal and the radiation–conduction interaction parameter defined by $a_s' r_c'$ and $\sigma' T_m'^3 r_c'/k_l'$, respectively. In the present work, the optical absorption coefficient of crystal a_s' is independent of the wavelength since we are considering the radiative heat transfer in gray absorbing–emitting media, and the melt is assumed to be opaque. n_s is the refractive index of the crystal and does not depend on

temperature. J is the irradiance defined by the zeroth-order moment of radiant intensity I, i.e.,

$$J = \int_{\omega=4\pi} I \,\mathrm{d}\omega. \tag{5}$$

The radiant intensity I is governed by the equation of transfer which represents the radiative heat transfer in an absorbing–emitting, nonscattering crystal. Here, to solve the radiative transfer equation, the FVM was used [11], where the 4π angular domain at any spatial location is divided into a finite number of discrete, M, nonoverlapping solid angles by the azimuthal discretization strategy. According to [11], the FVM is the same as the discrete ordinates method (DOM), except that the azimuthal discretization was used as the angular discretization strategy instead of the Sn-type one in the DOM. With the discretization of the angular domains, the radiative transfer equation along a specified discrete direction ω^m can be expressed as follows,

$$\frac{\mu^m}{r}\frac{\partial(rI^m)}{\partial r} - \frac{1}{r}\frac{\partial(\eta^m I^m)}{\partial \phi} + \xi^m \frac{\partial I^m}{\partial z} = -\kappa_s I^m + \kappa_s I_b. \tag{6}$$

Here, μ^m, η^m and ξ^m are the direction cosines along the cylindrical coordinates, and ϕ is the azimuthal angle measured from the r-direction. I_b is the blackbody radiant intensity at the temperature of the medium.

The boundary conditions for Eqs. (1),(2),(3),(4) and (6) are given by the following equations.

At the melt/crystal interface

$$T_l = T_s = 1, \tag{7a}$$

$$-\nabla T_l \cdot \boldsymbol{n}_{ls} + K_s \nabla T_s \cdot \boldsymbol{n}_{ls} = -PeSt(\boldsymbol{e}_z \cdot \boldsymbol{n}_{ls}) + N_R \sum_{m'}^{M} I^{m'} D^{m'} \omega^{m'}, \tag{7b}$$

$$I^m = n_s^2 \varepsilon_{ls} T_s^4 + \rho_{ls} \sum_{D^{m'}>0}^{M} I^{m'} D^{m'} \omega^{m'} \quad (D^m < 0). \tag{7c}$$

At the crystal surface

$$\nabla T_s \cdot \boldsymbol{n}_{sg} = 0, \tag{7d}$$

$$I^m = \tau_{sg}^{out} q_{i,s}^{out} + \rho_{sg}^{in} \sum_{D^{m'}>0}^{M} I^{m'} D^{m'} \omega^{m'} \quad (D^m < 0). \tag{7e}$$

At the material surfaces adjoining the surrounding gas

$$-K_j \nabla T_j \cdot \boldsymbol{n}_{jg} = \varepsilon_{jg}^{out} N_R (T_j^4 - q_{i,j}^{out}). \tag{7f}$$

At the interfaces between opaque materials

$$K_j \nabla T_j \cdot \boldsymbol{n}_{jk} = K_k \nabla T_k \cdot \boldsymbol{n}_{jk}. \tag{7g}$$

Here, St is the Stefan number defined by $\Delta H'_f / C'_{ps} T'_m$. In the CZ crystal growth system, each material constituting the furnace, such as the melt, the crystal and the crucible, is surrounded by a transparent gas, and the incident radiative heat flux to their surfaces through the ambient gas, i.e., irradiation q_i^{out}, is partially absorbed and reflected when the material is opaque. In the case of the semitransparent material, moreover, a part of the irradiation transmits inside the material. Thus, the boundary conditions for temperature and radiant intensity, Eqs. (7e) and (7f), include q_i^{out}. The superscripts "out" and "in" refer to the outside and inside of the surface adjoining the surrounding gas, respectively, and the subscript "i" of q_i^{out} implies the incident flux. In the present work, the melt/crystal interface and the crystal surface bounding the semitransparent crystal were assumed to be gray and to reflect diffusely.

To solve the governing equations with the boundary conditions, q_i^{out} should be given explicitly. Here, similarly to the previous work using the P_1 method [8], we first considered the gas phase in the CZ furnace shown in Fig. 1 as the enclosure surrounded by N opaque and semitransparent diffuse-gray surfaces of uniform temperature. Then, the irradiation onto a surface j, $q_{i,j}^{out}$, is given by the following equation, creating an energy balance with respect to the surface j in the enclosure,

$$q_{i,j}^{out} = \frac{1}{1-\rho_j^{out}} (\varepsilon_j^{out} T_j^4 + \tau_j^{in} q_{i,j}^{in} - q_j), \tag{8}$$

where q_i^{in} is the incident radiative heat flux on the inside of a semitransparent surface j, i.e., the crystal surface, and is expressed as

$$q_{i,j}^{in} = \sum_{D^{m'}>0} I^{m'} D^{m'} \omega^{m'}. \tag{9}$$

In addition, the net radiative heat flux at surface j, q_j in Eq. (8), is obtained as a solution of the following matrix equations which govern radiative heat transfer in the enclosure:

$$\left(\frac{1}{1-\rho_j^{out}}\right) q_j - \sum_{k=1}^{N} \frac{\rho_k^{out}}{1-\rho_k^{out}} F_{jk} q_k = \frac{1}{1-\rho_j^{out}} (\varepsilon_j^{out} T_j^4 + \tau_j^{in} q_{i,j}^{in}) - \sum_{k=1}^{N} \frac{1}{1-\rho_k^{out}} F_{jk} (\varepsilon_k^{out} T_k^4 + \tau_k^{in} q_{i,k}^{in}) \quad (j = 1, 2, \ldots, N), \tag{10}$$

where F_{jk} is the view factor which is calculated efficiently by combining the analytical solutions [10]. If the material with surface j is opaque, the transmissivity τ_j in Eqs. (8) and (10) is set to be zero, while the emissivity ε_j is neglected in the case of semitransparent materials.

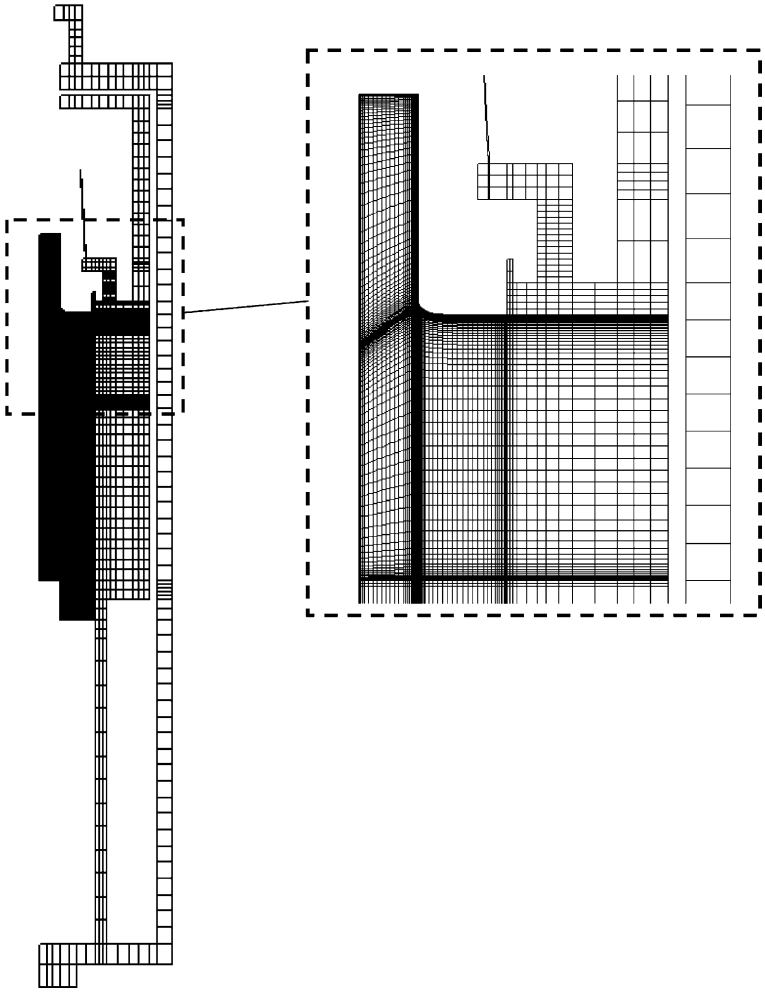

Fig. 2. Finite element discretization of the calculated domain.

The finite element method was used for the calculations of the temperature field in the furnace and velocity field in the melt, as well as the shapes of the melt/crystal and melt/gas interfaces. The calculation domain is discretized by 7631 isoparametric quadrilateral elements as shown in Fig. 2, and in each element, velocity vectors and temperature are approximated with bilinear polynomials and the pressure is considered to be constant. Also, to solve the radiative transfer equation, the spatial domain was discretized by the same number of control volumes as that of the finite elements in the crystal, while the 4π angular domain was divided into 3072 discrete solid angles. After the electromagnetic field in the CZ furnace and Q_0 in Eq. (3) are calculated for a reference value of current in the RF coil and the shape of the melt/gas interface is obtained, the global analysis is carried out according to the following procedure. (1) Eq. (10) is solved for the net radiative heat fluxes at the surfaces adjoining the ambient gas phase, q_j ($j = 1,2,\ldots,N$), with T_j and $q_{i,j}^{in}$ obtained in the previous step, and $q_{i,j}^{out}$ is obtained using Eq. (8). (2) Eq. (6) is solved for the radiant intensities in all discrete directions, I^m ($m = 1,2,\ldots,M$), and $q_{i,j}^{in}$ is re-calculated with Eq. (9). (3) Steps 1 and 2 are successively iterated until all equations and boundary conditions for the radiative heat transfer are satisfied. (4) The temperature and velocity fields in the furnace, the interface shape and α are simultaneously solved using q_i^{out} and I^m obtained in steps 1 to 3. (5) Steps 1 to 4 are repeated until all equations and boundary conditions are satisfied.

3. Results and discussion

Before investigating the effect of the radiative heat transfer within the crystal on the CZ crystal growth

process, it is important to ascertain the reliability and accuracy of the present simulation, i.e., the FVM used here. Therefore, the results of the simulation were compared with the following: (1) the exact solution for radiative flux along the lateral wall of a 2D axisymmetric triangular toroid, where the medium in the toroid with cold and black walls is maintained at an emissive power of unity and is assumed to be absorbing–emitting with $a' = 1.0\,\mathrm{m}^{-1}$ [11] and (2) the exact numerical solutions of the temperature profile in a gray gas contained between infinite parallel plates, where optical thickness of the gas is 1.0 and the plates are black at the dimensionless temperatures 0.5 and 1.0 [12]. Fig. 3(a) shows the calculated radiative wall flux distributions along the lateral wall of the triangular toroid using the FVM. Fig. 3(b) shows the calculated 1D temperature distributions in the gas between two black plates for the different values of the conduction–radiation parameter. The present numerical results were found to be in good agreement with the results in the literature.

Next, we consider the heat transfer in an inductively heated CZ furnace with 6 kHz radio-frequency current, as shown in Fig. 1, where a $LiNbO_3$ single crystal (22.8 mm diameter) is pulled continuously at the rate of $4\,\mathrm{mm\,h}^{-1}$ from the melt in a Pt crucible ($59.3\,\mathrm{mm}^{\mathrm{OD}} \times 62.7\,\mathrm{mm}^{\mathrm{H}} \times 1.1\,\mathrm{mm}^{\mathrm{T}}$). The physical properties of $LiNbO_3$ melt and crystal used in the calculations are identical to those used in our previous work [8,10]. In the present work, the effect of the absorption coefficient of the crystal on the heat transfer behavior in the CZ furnace and the melt/crystal interface shape is investigated, assuming the optical thickness of the crystal κ_s as a disposable parameter. In regard to the optical properties, the transmissivities on both sides of the semitransparent crystal surface are estimated with its refractive indices ($n_s = 2.3$) as [13,14]

$$\begin{aligned}\tau_s^{\mathrm{out}} &= 1 - \rho_s^{\mathrm{out}} \\ &= \frac{1}{2} - \frac{(3n_s+1)(n_s-1)}{6(n_s+1)^2} - \frac{n_s^2(n_s^2-1)^2}{(n_s^2+1)^3}\ln\left(\frac{n_s-1}{n_s+1}\right) \\ &\quad + \frac{2n_s^3(n_s^2+2n_s-1)}{(n_s^2+1)(n_s^4-1)} - \frac{8n_s^4(n_s^4+1)}{(n_s^2+1)(n_s^4-1)^2}\ln(n_s) \\ &\cong 0.80, \end{aligned} \tag{11a}$$

$$\tau_s^{\mathrm{in}} = 1 - \rho_s^{\mathrm{in}} = \frac{\tau_s^{\mathrm{out}}}{n_s^2} \cong 0.15. \tag{11b}$$

On the other hand, since the melt is opaque, the emissivity of the melt into the gas phase can be estimated to be 0.80 using Eq. (11a) for $\varepsilon_l^{\mathrm{out}} (= 1 - \rho_l^{\mathrm{out}})$, and also the emissivity into the crystal is 1.0 if n_l is assumed to be equal to n_s. The Prandtl number Pr and the Grashof number Gr $(= \beta' T'_m g' r'^3_c / \nu'^2_l)$ in this system are 13.6 and 4.67×10^5, respectively.

Fig. 4 shows the effect of the optical thickness κ_s on the temperature distributions in the furnace and the flow pattern in the melt for crystal rotational Reynolds number, Re $(= r'^2_c \Omega' / \nu'_l) = 200$. The stream functions in the figures are scaled with $r_c \nu'_l$. The figures show that the temperature gradients in the crystal decrease when the optical thickness decreases, because the contribution of the radiation to the total heat transfer through the crystal increases and the role of the thermal conduction diminishes. The larger heat flux due to the radiation through the crystal brings about the larger heat flux to the melt/crystal interface from the melt to compensate for it. Consequently, the power of the RF coil becomes large, the maximum value of the melt temperature becomes higher, and the melt/crystal interface increases its area and becomes more convex toward the melt.

Fig. 5 shows the effect of Re on the temperature distributions in the furnace and the flow pattern in the melt for $\kappa_s = 0.1$. When the crystal is not rotated, i.e., $Re = 0$,

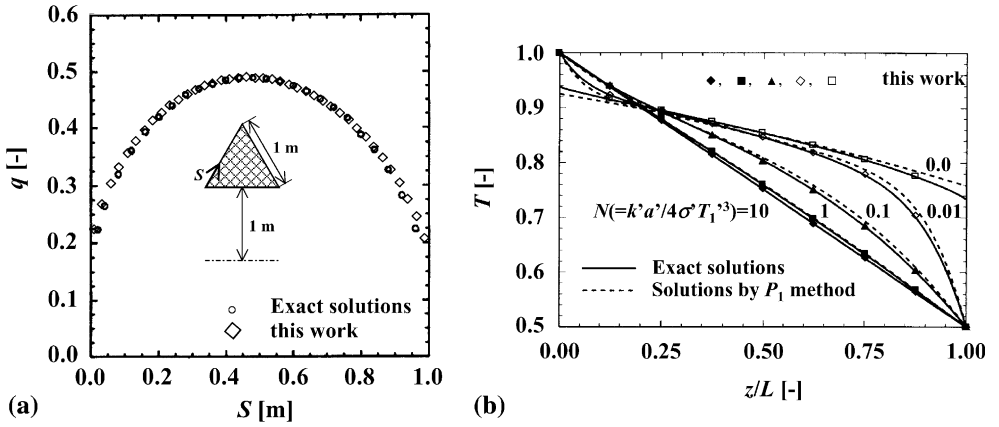

Fig. 3. (a) Calculated radiative wall flux distributions along the lateral wall of the triangular toroid. (b) Calculated 1D temperature distributions in the gas between two black plates.

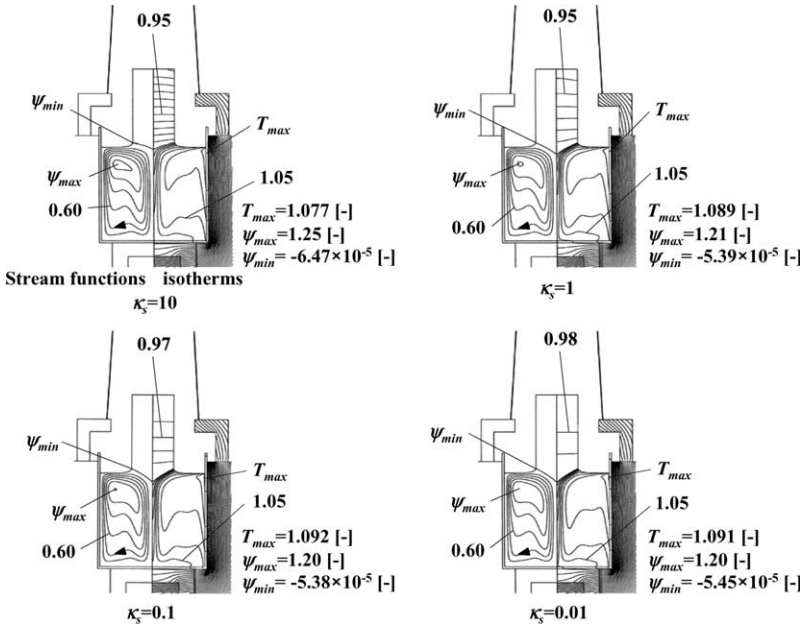

Fig. 4. Effect of the optical thickness on the temperature distributions in the furnace and the flow pattern in the melt for $Re = 200$, where $\Delta T = 0.01$ and $\Delta\psi = 0.2$.

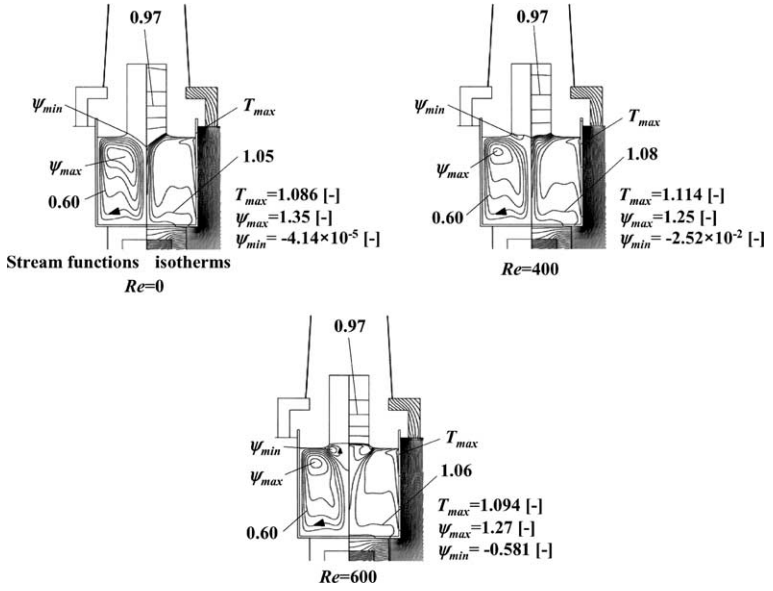

Fig. 5. Effect of Re on the temperature distributions in the furnace and the flow pattern in the melt for $\kappa_s = 0.1$, where $\Delta T = 0.01$ and $\Delta\psi = 0.2$.

only the clockwise vortex caused by free convection is present in the melt, and the flow pattern exhibits an undulating structure at the bottom of the crucible due to a retarding force caused by the vertical stratification of the melt. At $Re = 400$, a counterclockwise vortex due to crystal rotation appears under the crystal, in addition to free convection, and the melt/crystal interface is almost flat. Moreover, when the crystal rotation rate increases, i.e., $Re = 600$, the intensity of the vortex due to crystal rotation becomes strong and the melt/crystal interface becomes concave toward the melt. From the results, it is found that a melt convection

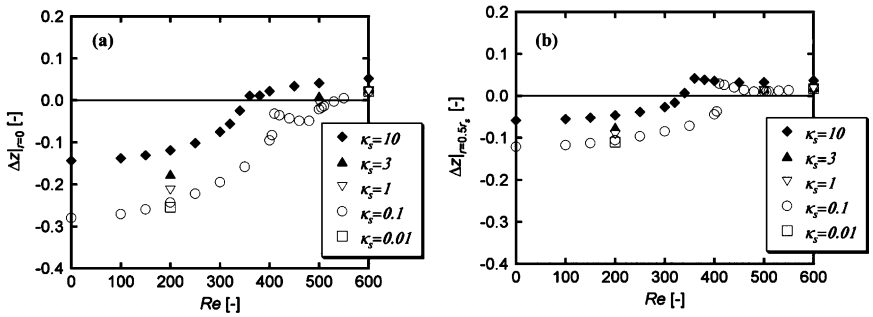

Fig. 6. Effect of the crystal rotational Reynolds number on the melt/crystal interface shapes.

affects the temperature distributions in the melt and crystal and consequently the melt/crystal interface shape because the Prandtl number of the oxide melt is relatively large (>1).

Fig. 6(a) and (b) show the effect of the crystal rotational Reynolds number Re on the melt/crystal interface shapes for the different values of optical thickness of the crystal. In these figures, $\Delta z|_{r=0}$ in (a) represents the axial displacement of the interface at the centerline from the axial position of the melt/crystal/gas tri-junction ($r = r_s$), and $\Delta z|_{r=0.5r_s}$ in (b) denotes the axial displacement at the half position of the crystal radius. When both $\Delta z|_{r=0}$ and $\Delta z|_{r=0.5r_s}$ are negative, the interface shape is completely convex toward the melt. When κ_s=10 and 0.1, $\Delta z|_{r=0}$ and $\Delta z|_{r=0.5r_s}$ increase with Re, and the melt/crystal interface shape changes from convex to a doubly curved or 'gull-wing' geometry, and then becomes completely concave toward the melt as shown in Fig. 5, where the doubly curved interface corresponds to the case that satisfies the following relations, $\Delta z|_{r=0} < \Delta z|_{r=0.5r_s}$ and $\Delta z|_{r=0.5r_s} > 0$. Fig. 6 demonstrates numerically that the interface inversion occurs with the increase of Re. When Re is relatively small and the interface is convex toward the melt, the magnitude of the interface deflection $\Delta z|_{r=0}$ becomes larger as the optical thickness of the crystal κ_s decreases, and consequently Re_c shifts to a larger value, where Re_c is the critical Reynolds number defined as Re at which $\Delta z|_{r=0}$ becomes a positive value, i.e., the interface inversion occurs. In addition, the dependences of $\Delta z|_{r=0}$ and $\Delta z|_{r=0.5r_s}$ on Re near Re_c become more marked, and thus the interface changes more abruptly. These steep increases of $\Delta z|_{r=0}$ and $\Delta z|_{r=0.5r_s}$ are due to the melt flow toward the melt/crystal interface caused by the crystal rotation. However, as Re increases beyond Re_c, the center of the vortex of the forced convection by the crystal rotation moves toward the outside, and the sequential melt flow directs a radially uniform heat flux to the interface and thus flattens it. Hence, the difference between $\Delta z|_{r=0}$ and $\Delta z|_{r=0.5r_s}$ for the same Re and their dependences on Re become smaller.

4. Conclusions

For the single crystal growth of an oxide, the global analysis of heat transfer in the inductively heated CZ furnace was carried out in order to investigate the effect of optical properties of crystal on the CZ crystal growth process. Here, the P_1 method used in previous works was replaced with the FVM to solve the radiative transfer equation, so that even the crystal with a relatively thin optical thickness could be accounted for. As a result, it was found that the melt/crystal interface becomes more convex toward the melt for a small rotational Reynolds number as the optical thickness decreases. In addition, the critical Reynolds number, at which the interface inversion occurs, decreases with the optical thickness of the crystal.

References

[1] B. Cockayne, M. Chesswas, D.B. Gasson, Facetting and optical perfection in Czochralski grown garnets and ruby, J. Mater. Sci. 4 (1969) 450–456.
[2] Ji. Kvapil, Jo. Kvapil, B. Manek, B. Perner, R. Autrata, P. Scuer, Czochralski growth of YAG:Ce in a reducing protective atmosphere, J. Cryst. Growth 52 (1981) 542–545.
[3] C.D. Brandle, V.J. Fratello, A.J. Valentine, S.E. Stokowski, Effects of impurities and atmosphere on the growth of Cr-doped gadolinium scandium gallium garnet. I, J. Cryst. Growth 85 (1987) 223–228.
[4] Y. Okano, Y. Tsuji, D.H. Yoon, K. Hoshikawa, T. Fukuda, Internal radiative heat transfer in Czochralski growth of $LiTaO_3$ single crystal, J. Cryst. Growth 141 (1994) 383–388.
[5] Q. Xiao, J.J. Derby, The role of internal radiation and melt convection in Czochralski oxide growth: deep interfaces, interface inversion, and spiraling, J. Cryst. Growth 128 (1994) 188–194.
[6] Q. Xiao, J.J. Derby, Heat transfer and interface inversion during the Czochralski growth of yttrium aluminum garnet and gadolinium gallium garnet, J. Cryst. Growth 139 (1994) 147–157.
[7] I.Y. Evstratov, S. Rukolaine, V.S. Yuferev, M.G. Vasiliev, A.B. Fogelson, V.M. Mamedov, V.N. Shlegel, Y.V.

Vasiliev, Y.N. Makarov, Global analysis of heat transfer in growing BGO crystals ($Bi_4Ge_3O_{12}$) by low-gradient Czochralski method, J. Cryst. Growth 235 (2002) 371–376.
[8] M. Kobayashi, T. Hagino, T. Tsukada, M. Hozawa, Effect of internal radiative heat transfer on interface inversion in Czochralski crystal growth of oxides, J. Cryst. Growth 235 (2002) 258–270.
[9] M. Kobayashi, T. Tsukada, M. Hozawa, Effect of internal radiation on thermal stress fields in CZ oxide crystals, J. Cryst. Growth 241 (2002) 241–248.
[10] T. Tsukada, M. Hozawa, N. Imaishi, Global analysis of heat transfer in CZ crystal growth of oxide, J. Chem. Eng. Jpn. 27 (1994) 25–31.
[11] J. Liu, H.M. Shang, Y.S. Chen, Development of an unstructured radiation model applicable for two-dimensional planar, axisymmetric, and three-dimensional geometries, J. Quant. Spectrosc. Radiat. Transfer 66 (2000) 17–33.
[12] M.F. Modest, Radiative Heat Transfer, McGraw-Hill, New York, 1993, pp. 713–724.
[13] C.M. Spuckler, R. Siegel, Refractive index effects on radiative behavior of a heated absorbing–emitting layer, J. Thermophys. Heat Transfer 6 (1992) 596–604.
[14] C.M. Spuckler, R. Siegel, Refractive index and scattering effects on radiation in a semitransparent laminated layer, J. Thermophys. Heat Transfer 8 (1994) 193–201.